

ALMA MATER STUDIORUM · UNIVERSITY OF BOLOGNA



School of Science
Department of Physics and Astronomy

Measurement of Muon Lifetime

Supervisors:

Prof. Luigi Guiducci
Dott. Marco Garbini
Dott. Federica Primavera
Dott. Marco Selvi

Submitted by:

Danish Alam
Robin Pelkner
Daniele Rossi

Academic Year 2021/2022

Abstract

In this experiment, we studied cosmic muon decays using plastic scintillator detectors. We aimed to obtain the muon lifetime by stopping the muon and measuring its decaying at rest to an electron. The experimental signature was given by a signal from the muon decay, followed by a delayed signal coming from the electron. We selected muon event candidates and subsequently identified events with a clear sign of their decaying. Muon lifetime is obtained from a fit to their decay time distribution. We also discussed the experimental setup and detection techniques, taking data and analysing these data to estimate the muon lifetime. The muon lifetime was measured to be $2.1 \pm 0.1 \mu\text{s}$. Also an attempt to calculate the lifetime of captured muons in iron was made.

Contents

| | | |
|----------|--|-----------|
| 1 | Introduction | 1 |
| 1.1 | General introduction to muons | 2 |
| 1.2 | Muons from cosmic ray showers | 2 |
| 2 | Experimental Setup | 4 |
| 3 | Preliminary Measurements | 7 |
| 3.1 | Working Voltage for the Photomultipliers | 7 |
| 3.2 | Threshold measurements | 8 |
| 3.3 | Delay Curve | 10 |
| 3.4 | TDC calibration | 11 |
| 4 | Trigger Logic and Data Taking | 13 |
| 5 | Data Analysis | 16 |
| 5.1 | Data selection and background | 16 |
| 5.2 | Fit function | 17 |
| 5.3 | Fit results | 18 |
| 5.4 | Decay of captured muons | 20 |
| 6 | Final Results and Conclusions | 22 |
| A | Threshold voltages of the PMTs | 24 |
| B | TDC calibrations | 28 |

Chapter 1

Introduction

This experiment aims to determine the lifetime of muons. Muons are produced by cosmic ray showers in the higher atmosphere. Incoming Protons interact with the atmosphere and produce pions, which can decay into muons that are reaching the surface of the earth.

In this experimental setup, the incoming muons are slowed down and stopped by layers of iron and then detected with plastic scintillators.

This report is structured as follows: in this chapter, an introduction to the physical aspects of muons is given. Chapter 2 describes the used components and the experimental setup. In Chapter 3 the preliminary measurements for the calibration of the setup are described and their results are discussed. Chapter 4 discusses the composition of the experiment and the process of data taking, while Chapter 5 presents the data analysis. Chapter 6 concludes this report.

1.1 General introduction to muons

The standard model of elementary particles differentiates between quarks, leptons, and bosons. Quarks, as well as leptons, can be divided into three generations. The muons and the antimuon respectively are the second generation of leptons together with their associated neutrinos. Like the electron, muons have spin 1/2 and a negative elementary charge (a positive elementary charge for the antimuon). Although the similarities, they differ concerning their masses and their lifetimes.

While the electron is a stable particle, the muon has a finite lifetime, which this experiment is supposed to measure. The lifetime, given as an average result of past measurements, is $\tau = (2.196\,981\,1 \pm 0.000\,002\,2) \mu\text{s}$. Their mass is $m_\mu = (105.658\,374\,5 \pm 0.000\,002\,4) \text{ MeV}$, which is 206 times the mass of the electron [6].

1.2 Muons from cosmic ray showers

Muons are naturally produced in cosmic ray showers. The cosmic ray is mostly protons, but also electrons and atomic nuclei. These particles originate in various galactic and intergalactic sources like the sun, the Milky Way, and other galaxies. When a cosmic particle (e.g; Proton) strikes and interact the atmosphere, it produces a hadronic shower. The protons hadronize mostly into π mesons, because they are the lightest mesons, but also into K mesons and other hadrons. Due to their short lifetimes, Pions and Kaons also decay into muons via the weak interaction.

$$\begin{aligned}\pi^+ &\rightarrow \mu^+ + \nu_\mu \\ \pi^- &\rightarrow \mu^- + \bar{\nu}_\mu.\end{aligned}$$

This process is analogous to K mesons. The muons also only decay via the weak interaction as follows

$$\begin{aligned}\mu^- &\rightarrow e^- + \bar{\nu}_e + \nu_\mu \\ \mu^+ &\rightarrow e^+ + \nu_e + \bar{\nu}_\mu.\end{aligned}$$

Because the muons have a longer lifetime than pions. Hence, muons can reach the surface of the earth and can be detected through their decay. A schematic with typical processes, which lead to the production of muons, can be seen in Figure 1.1.

Once they arrive on the surface of earth, we can use experimental apparatus to detect them. The basic idea is that when a particle passes through matter they release part of its energy which is converted into new particles or radiation. The amount of released energy is described by the Bethe Bloch Formula:

$$-\frac{dE}{dx} = 2\pi N_a r_e^2 m_e c^2 \rho \frac{Z}{A} \frac{z^2}{\beta^2} \left[\ln\left(\frac{2m_e \gamma^2 v^2 W_{max}}{I^2} - 2\beta^2 - \delta 2 \frac{C}{Z}\right) \right]$$

The transferred energy from the particle to the atom will cause ionization or excitation of scintillating materials which convert these energies into visible lights. Then these visible light signals are converted into the electronic signals using the Photomultiplier tubes.

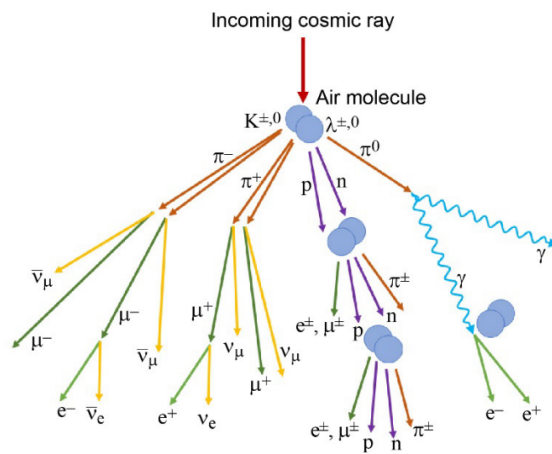


Figure 1.1: Typical shower processes after an incoming cosmic ray. The primary rays induce secondary particles by scattering with the molecules of the atmosphere. These secondaries can decay or scatter again with the atmosphere and produce more particles in the process. This is called a decay chain or a cosmic ray shower[5].

Chapter 2

Experimental Setup

In our experiment, we are detecting, mostly cosmic muons slowed by iron block(26 cm thick), using three layers of plastic scintillators (P0, P1 and P2) coupled to photo multipliers tubes (PMTs) each via a light guide. Due to the mechanisms of energy loss, from Bethe-Bloch formula, the minimum energy needed by muons to pass through 26 cm of iron is $E_\mu \approx 382\text{MeV}$ (considering muons at the minimum of ionization energy). Moreover, the block of iron reduces the electromagnetic component of the cosmic rays. The incoming muons are detected by the counters P0 and P1 which are thin enough to allow the muons to pass through. During the passage, these charged muons excite the vibrational motion of the molecules which, when de-energized, emit visible light photons(1 photon for every 100 eV deposited). The number of photons produced by scintillation is proportional (within statistical considerations) to the energy loss of the passing particle. Those photons will enter the PMT and produce electrons that form the electrical pulse we measure. The size of electronic pulse in a PMTs is proportional to the number of photons produced by scintillator. To maximize the numbers of photon that reach the photocathode of the PMTs, it is necessary that the scintillator, light guide and photomultiplier tube all be wrapped in reflective foil. Also, to block external light the assembly is then covered by black tape. After P1, the muons encounter a slab of iron in which some of them eventually stop and decay. If it happens, the emitted electron or positron is then detected by the surrounding counters. Therefore, what we would like to measure is the time interval between the signal for a stopped muon (' μ stop') and the detection of emitted electron or positron.

Other than the detector itself, we use a NIM (Nuclear Instrument Modules) and a CAMAC (Computer Automated Measurement And Control) crate with appropriate boards and modules. All algorithms and tunings of the experiment are done within the NIM crate and CAMAC is used for the read-out. The NIM modules which are used can be summarized as follows:

HV power supply:

N470 CEAN 4 Channel NIM Programmable High Voltage Power Supply.

This module is the power supply to the photomultiplier tubes.

Discriminator:

N840 CEAN 8 Channel Leading Edge Discriminator module; pulse width: 5-40 ns, and threshold 1-255 mV.

Given an analog input signal, the discriminator compares the amplitude with a threshold (in mV since it is amplitude). If the falling edge of the input signals overcomes the threshold then a LOGIC 1 signal is

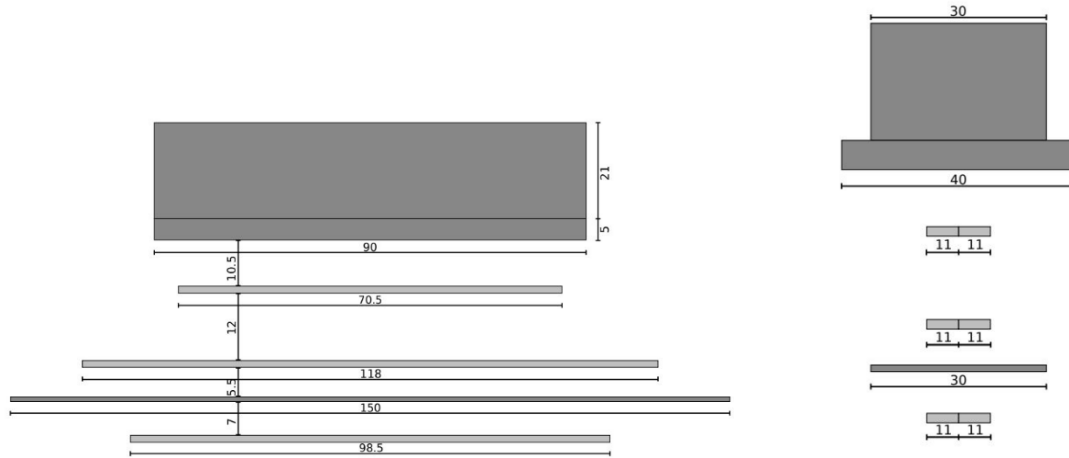


Figure 2.1: The experimental setup where it is shown in lateral and front view the absorber layers (dark grey) and the scintillator planes (light grey) with the dimensions in cm. Ref. Lab Manual Part 1

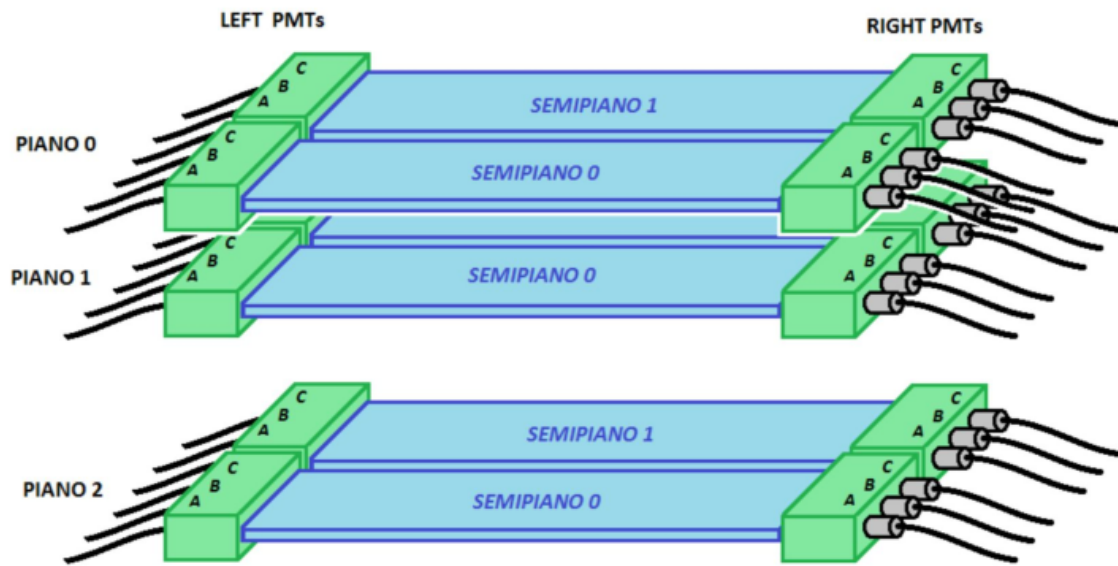


Figure 2.2: Scintillators with PMTs arranged in planes. Ref. Lab Manual Part 1

produced as output. If the signal is lower than the threshold, a LOGIC 0 is generated. The Standard LOGIC used by this module is the Nuclear Instrument Module Logic (NIM).

Logic Unit:

CAEN N405 3-fold logic unit module having 3 independent sections to perform logic AND/OR up to 4 logic signals in input.

It provides 1 linear OUT (width of the signals depending on input signals superposition), 2 fixed width (adjustable) OUT signals, 1 ANTI OUT signal, and 1 VETO input.

The first signal enters the LOGIC unit. During this time it is “1” the other signal arrives so there is Δt during which both signals are “1”. This means the signals coincide and an AND signal is produced.

FI/FO:

CAEN N625 Quad Linear FAN-IN FAN-OUT module

The module has 4 identical sections. Each section has 4 inputs that can be fed with analog signals. Then for each section, there are 4 identical OUT signals. If only one IN is used the 4 OUT are the replica of the IN signal. If more than one IN is connected then the OUTs provide the sum of the IN signals. So each of the 4 sections of this module can be used to replicate a signal 4 times (4 OUT).

Counter/Scaler:

CAEN N1145 Quad Scaler and Preset Counter/Timer

Count 4 NIM or TTL level signals for a given time interval defined by the user. The user can follow the countdown and read the number of counts on displays.

Dual Timer:

CEAN N93B Dual Timer module

This NIM module housing two identical triggered pulse generators which produce NIM and ECL pulses whose width ranges from 50 ns to 10 s when triggered. Output pulses are provided normal and complementary. Timers can be re-triggered with the pulse end marker signal.

Dual Delay:

CEAN N108A Dula delay module

Delay ranges from 0 to 63.5 ns (+ 1.6 ns offset) per section. The delay can be set in 0.5 ns steps. The delay lines are made up of calibrated coaxial cable stubs for high accuracy delay and do not require power supply.

Oscilloscope:

TDC:

CAEN mod. C414

A single width CAMAC unit housing 8 independent 12 bit time-to-digital conversion channels. The full scale time can be selected from 100 ns to 5 s via internal DIP switches. The time resolution ranges from 25 ps to 1.25 ns (respectively for 100 ns and 5 s full scale time range). The conversion time is 2.5 s per channel and it is reduced to 1.5 s for overflow channels. A CAMAC LAM is generated (if enabled) at the end of the conversion.

Chapter 3

Preliminary Measurements

3.1 Working Voltage for the Photomultipliers

As a first step, the optimal working voltages for the photomultipliers (PMTs) have to be found. Two PMTs were chosen for this measurement as a sample from the whole detector, R10B and R20A. It is important to choose PMTs from different planes to make sure the measured signal is due to a particle crossing the detector. A schematic for the measuring circuit is shown in Figure 3.1.

Only signals measured with both PMTs are taken into account. To determine these coincidences logic

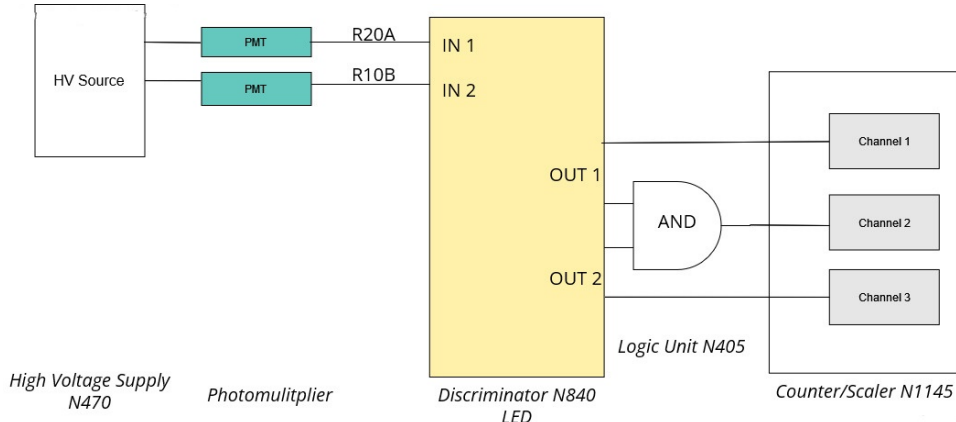


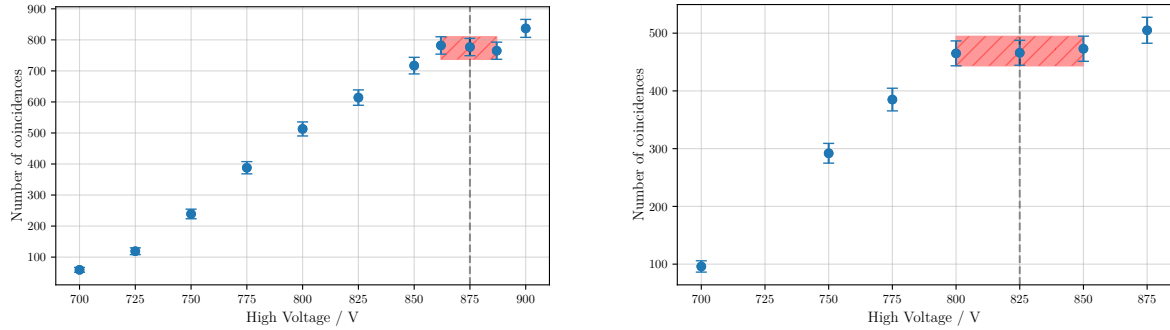
Figure 3.1: Schematic representation of the coincidence counting circuit for the PMTs. The signal propagation is from left to right starting with the PMTs and their high voltage supply and ending with the scaler.

signals are needed and for this, discriminators with a threshold of 40 mV are used. They convert the analogous signals of each PMTs into NIM standard signals. Using a logic unit module, we get the coincidences from the logic AND of both PMT signals. The NIM signals last for 40 ns each so the signals do not have to arrive at the same time but within 40 ns of each other because the muons arrive in the different planes at different times and not necessarily at the same distance from the PMTs. Furthermore,

the PMTs may have different delay times as well.

For the measurement, the R10B PMT works on a fixed high voltage of 775 V while the high voltage of R20A is varied from 700 V to 900 V. Each measurement lasts 200 s. The taken data is shown in Figure 3.2. A plateau can be found with 875 V corresponding to the middle value of it. This value is used as a fixed value for the R20A PMT when the voltage of the R10B PMT is varied in the same range of high voltages. The measurements for this PMT were each taken in 100 s due to time limitations. The central value of the plateau for this PMT is 825 V. Both measurements were also stopped when the PMTs are operating in the discharge region due to the high voltage to avoid damaging the PMTs.

The results are shown in Figure 3.2a and Figure 3.2b. All uncertainties are obtained assuming a Poissonian distribution, meaning $\sigma \propto \sqrt{N}$, where N is the number of coincidences. Because the output of the high voltage sources can fluctuate, the central values of the plateaus, 875 V for the R20A PMT and 825 V for the R10B PMT, can be used as the optimal working voltages to ensure a voltage output in the region of the plateau.



(a) Data of the R20A PMT. The central value of the plateau is 875 V.

(b) Data of the R10B PMT. The central value of the plateau is 825 V.

Figure 3.2: Measured number of coincidences regarding varying high voltages of the R10B PMT and the R20A PMT. The dashed line indicates the central values of each plateau. The striped red areas mark the found plateaus.

3.2 Threshold measurements

After the optimal working voltages was found, the determination of the optimal threshold voltage of the chosen PMTs started. A good determination of the threshold is necessary to suppress electronic noise on the one hand, but also to make sure that real signals are not filtered as well on the other hand. So the threshold can neither be too low nor too high.

Similar to the step before, a counting experiment of coincidences concerning the threshold voltages is conducted. This time the circuit arrangement is shown in Figure 3.3 is used. The PMTs are powered using the working voltages given in the laboratory as an average optimal working voltage for three PMTs.

In principle, the threshold of the discriminator of one plane is kept fixed at 15 mV, while the threshold of the other discriminator is being varied from 5 mV to 250 mV in irregular steps. Using a discriminator and

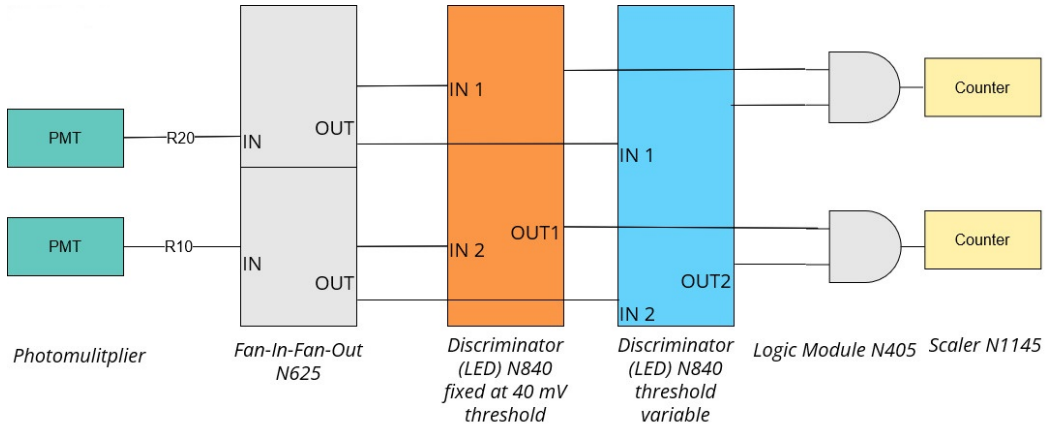


Figure 3.3: Schematic representation of the electronic circuit used to find the optimal threshold voltage .The signal flows from left to right, starting with the PMTs and Ending with the scaler.

a Fan-in-Fan-out system as shown in Figure 3.3, it is possible to vary the threshold of the discriminators of both PMT planes at the same time. Each counting measurement was conducted in 60 s.

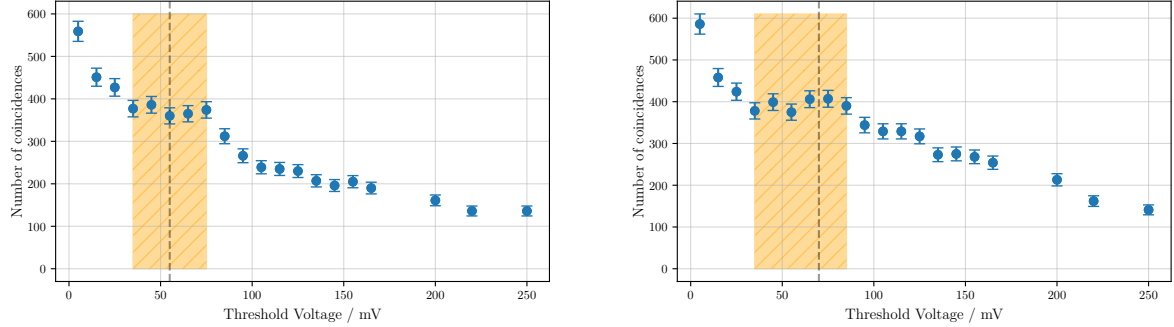
The results for the R10 and R20 planes can be seen in Figure 3.4. Results from other planes have to be taken from Appendix A, figures Figure A.1 to Figure A.6.

The data shows a higher number of coincidences at low threshold voltages, which decreases with

Table 3.1: Overview of optimal threshold voltages for each plane.

| Plane | Voltage / mV | Plane | Voltage / mV | Plane | Voltage / mV |
|------------|--------------|------------|--------------|-------|--------------|
| R00 | 50 | R20 | 55 | L01 | 55 |
| R10 | 70 | R21 | 55 | L11 | 75 |
| <i>R10</i> | 45 | L00 | 30 | L20 | 50 |
| R01 | 55 | L10 | 35 | L21 | 50 |
| R11 | 60 | <i>L10</i> | 60 | | |

rising voltages. This behavior is the same for all PMTs although not all curves show it that clearly. Also, a plateau of optimal threshold voltages can be seen. From the middle of this plateau, a threshold voltage has to be chosen as the optimal threshold value. As before the uncertainties will be taken into consideration using the Poissonian error. The optimal threshold voltages of all PMTs are shown in Table 3.1. Note that for the L10 signals and the R10 signals two measurements were taken. Thus, in these cases, only the value from the curve where it is easier to detect where the plateau is will be taken into consideration. The other values are marked italic in the tabular.



(a) Data of the R20 PMTs. The central value of the plateau is 55 mV.

(b) Data of the R10 PMTs. The central value of the plateau is 70 mV.

Figure 3.4: Measured number of coincidences concerning varying threshold voltages of the R10 PMTs and the R20 PMTs. The dashed line indicates the central values of each plateau. The striped orange areas mark the found plateaus.

3.3 Delay Curve

With systematical variation of the delay between the PMTs R10 and R20 a delay curve for these PMTs can be created. This delay curve is shown in Figure 3.5. For this measurement delay is added to the signals and the coincidences are counted using scalers in a 60 s timeframe. With the usage of a Fan-In-Fan-Out module the same delay can be applied to both signals at the same time.

The delay curve describes the number of coincidences measured for various delays between the PMTs. A negative delay time indicates a delay for the signal of R10, while a positive delay represents a delay of the signal of R20. The flanks of the curve can be fitted with linear functions of the form

$$N(\Delta t) = a \cdot \Delta t + b$$

with N as the number of coincidences and Δt as the delay time. The parameter are

$$a_{\text{left}} = (64.9 \pm 7.6) \frac{1}{\text{ns}} \quad b_{\text{left}} = 2328.6 \pm 251.4$$

for the left flank from -36 ns to -25 ns and

$$a_{\text{right}} = (-49.4 \pm 6.3) \frac{1}{\text{ns}} \quad b_{\text{right}} = 1972.6 \pm 227.3$$

for the right flank in the interval 32 ns to 40 ns. The plateau between the two flanks has an average value of 343.3 ± 18.6 . With the estimated parameters and the plateau value the time values of the half maximums are

$$\Delta t_{\text{left}} = -33 \pm 5 \quad \Delta t_{\text{right}} = 36 \pm 7.$$

Thus, the full width half maximum can be estimated as

$$\Delta t_{\text{FWHM}} = 70 \pm 9$$

which is a measure for the resolution of the PMTs.

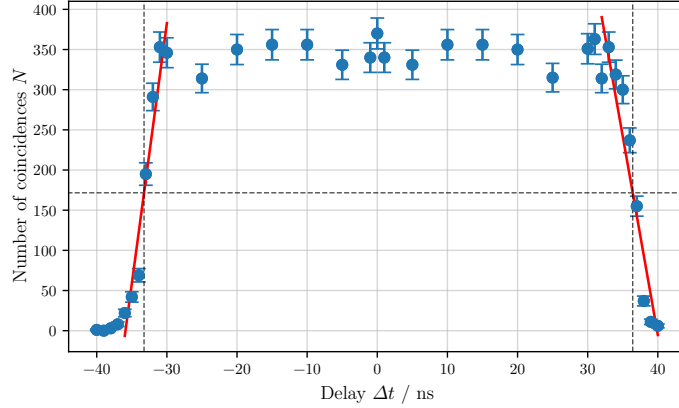


Figure 3.5: Delay Curve between the PMTs R10 and R20. The number of coincidences is plotted against the delay between the the PMTs. Furthermore, linear fits of the flanks and the FWHM are plotted.

3.4 TDC calibration

To convert the TDC time units into real time units the various TDC channels have to be calibrated. In this step malfunctioning TDC channels can be detected as well. To accomplish this, a fake trigger signal is needed at a rate of about 4 Hz. A fake signal is used to optimize the shape and the rate for an optimal calibration measurement. The fake signal is generated using the end marker of a dual timer. First, a signal is send to the START of the TDCs. Then this signal is used to create a delayed signal which stops the various channels. The time difference between start and stop signal was measured with an oscilloscope. To ensure a good calibration, all cables had to be of the exact same length.

For all channels and for each time difference ranging from $0.5 \mu s$ to $4.8 \mu s$ at least 200 measurements have been done. Special attention had to be given to the TDC channels which generated an overflow (i.e. a value greater than 4095) and other anomalies. These channels could not be fully used in the data taking since they would provide unreliable and incomplete data. Especially the second TDC had problems regarding overflows at times greater than $3 \mu s$.

For all channels a linear function of the form

$$\text{TDC Time} = a \cdot t + b$$

is fitted to the data, where t represents the real time values. These are shown for all channels in the figures B.1 to B.8 in Appendix B. The estimated parameters are shown in Table 3.2. Furthermore, a χ^2 -test is conducted for all fits, although it has to be taken into account that for some fits a cut-off due to overflow of the time values had to be done. The results of χ^2 -test per degree of freedom and the cut-off values are also shown in the table.

With the cut-off of overflow values the χ^2 -test values of the fits of all channels are small with the biggest value being produced in channel 2 of TDC 2, which will not be used due to its cut-off anyway. Thus, the fits can be considered successful. For the data acquisition the channels 3, 4, 5 and 6 of both TDCs have been chosen. In the data analysis both parameter will be used to convert the TDC times into real times although the offset b being small in comparison to the common TDC times ranging from 0 to 4095.

Table 3.2: Parameters of the fits for the TDC calibration with cut-off values and χ^2 values of the fits.

| Channel | Slope a / TDC Units/ns | Offset b / ns | cut-off / μs | $\chi^2/\text{d.o.f.}$ |
|---------|--------------------------|-----------------|-------------------------|------------------------|
| TDC 1 | | | | |
| 1 | 0.754 ± 0.001 | 10 ± 5 | - | 0.037 |
| 2 | 0.766 ± 0.001 | 6 ± 5 | - | 0.038 |
| 3 | 0.747 ± 0.001 | 10 ± 5 | - | 0.037 |
| 4 | 0.758 ± 0.001 | 10 ± 5 | - | 0.037 |
| 5 | 0.738 ± 0.001 | 11 ± 4 | - | 0.036 |
| 6 | 0.719 ± 0.001 | 10 ± 4 | - | 0.035 |
| 7 | 0.732 ± 0.001 | 12 ± 4 | - | 0.034 |
| 8 | 0.742 ± 0.001 | 12 ± 4 | - | 0.035 |
| TDC 2 | | | | |
| 1 | 0.808 ± 0.001 | 44 ± 6 | 4.6 | 0.053 |
| 2 | 0.943 ± 0.005 | 48 ± 10 | 3.5 | 0.120 |
| 3 | 0.802 ± 0.002 | 37 ± 6 | 4.6 | 0.056 |
| 4 | 0.791 ± 0.002 | 43 ± 5 | 4.7 | 0.048 |
| 5 | 0.783 ± 0.001 | 15 ± 5 | - | 0.042 |
| 6 | 0.786 ± 0.001 | 29 ± 5 | 4.7 | 0.042 |
| 7 | 0.813 ± 0.002 | 44 ± 6 | 4.5 | 0.062 |
| 8 | 0.802 ± 0.002 | 39 ± 6 | 4.6 | 0.057 |

Chapter 4

Trigger Logic and Data Taking

The trigger system that we need is a logic circuit that will be able to select muons that do not cross the setup. Thus, we can retrieve a signal of a stopping muon that can be used as a start signal for the time measurement of the decay. If we take Figure 2.2 as reference of the experimental apparatus each of the half-planes of plane 0 have two PMTs, which will be connected with an AND gate. The two half-planes with an OR gate in this way only the signal that activate the two PMTs can enter the circuit as can be seen in Figure 4.1. By doing this, we avoid detecting too much background. Meanwhile the OR gate is needed since there are two half-planes and a muon can cross either two.

We repeat the process for plane 1. For plane 2 we want a NOT gate at the end of the OR gate, so that

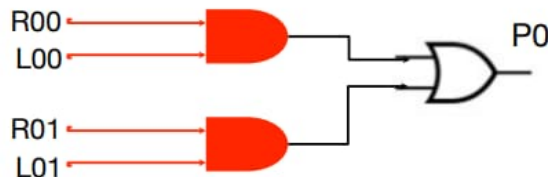
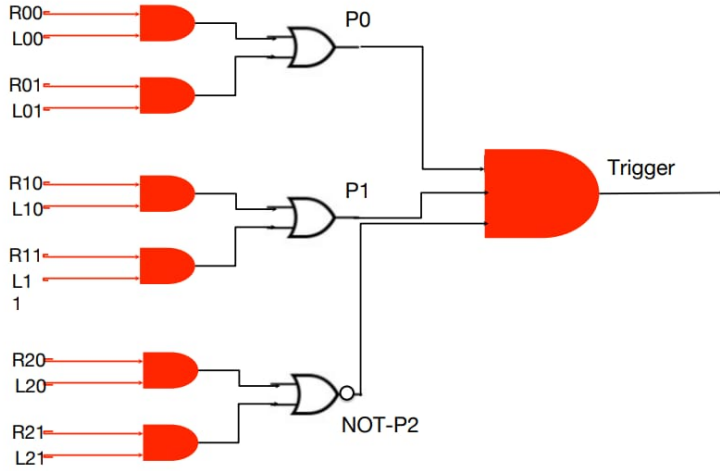


Figure 4.1: Logic circuit of plane 0.

we have a signal when no muons cross P2 to make sure that the muon has actually stopped. The P0, P1 and NOT P2 will be connect to an AND gate so that only when all of them generate a signal we can have the Trigger signal as shown in Figure 4.2.

For the time measurement we use a couple of TDCs in series since we need a least 10 μs and the max time measurable for this TDC is 5 μs . The TDC is controlled by a crate controller that sends the information from the module. The crate controller works with a DAQ code (labview) that creates memory location that will be read by the crate which will give command to the CAMAC module in this way

1. if and only 1 of the clock of the TDC has a stop before the time limit (5 μs) then a memory location called LAM is set to 1
2. the crate read continuously the memory location of the LAM, if it's 1 the crate controller stops the reading the LAM read the measurement and then clear them to start again

**Figure 4.2:** Trigger system.

The problem is that if there are no stopping signal the LAM wil never be set to 1 and we have a DAQ hanging problem. The solution is given by taking a copy of the start signal dealy it by $4.7 \mu\text{s}$ and connect it to one of the clock in this way we have a fake stop to prevent the problem. With this in mind we build the circuit shown in Figure 4.3.

The first three clocks will be connected to the P0, P1 and P2 in search for an electron apparence signal. The start for the first TDC in given by the trigger and then we take a copy of it and delay it by $4.7 \mu\text{s}$ (q1). From this we take 3 copy with a fan-in-fan-out :

1. the first will be used as the fake stop for the first TDC (q2)
2. the second will be the start of the second TDC
3. the third will be delayed again by a time $< 5 \mu\text{s}$ and used as a fake stop for the second TDC (q3)

The last thing is to make sure that no trigger is generated in the deadtime of the DAQ so we take the signal enlarge it up to $100 \mu\text{s}$ and send back to the logic unit that provide the trigger in the VETO input (e1).

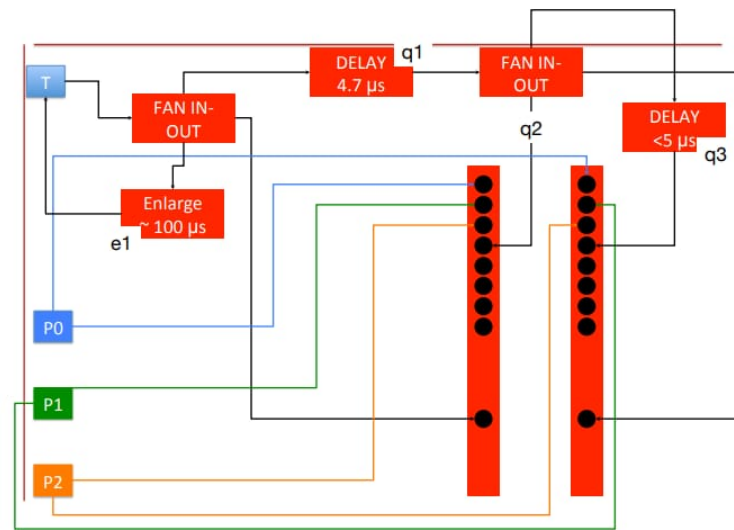


Figure 4.3: Data aquistion circuit.

Chapter 5

Data Analysis

5.1 Data selection and background

The data analysis was conducted using Python 3.7. Since the amount of taken data is high and only a few events have to be selected the *Pandas* package [3] is used to store and handle the data efficiently. The selection is necessary due to low signal rate in comparison to a high background rate. Measured trigger signals are not always electron signals from the muon decay. Since the experimental setup is positioned inside a building and shielded with a block of iron most of the signals can be assumed to originate from muons, since muons are the most penetrating particles. Still, there can be false signals for a variety of reasons.

As described in chapter 4 when a muon is stopped by the thinner iron block and thus only produces a signal in P0 and P1. However, depending on the incoming angle of the muon, a muon can be regarded as stopped even though it is not due to the geometry of the experiment as shown in Figure 5.1. In this

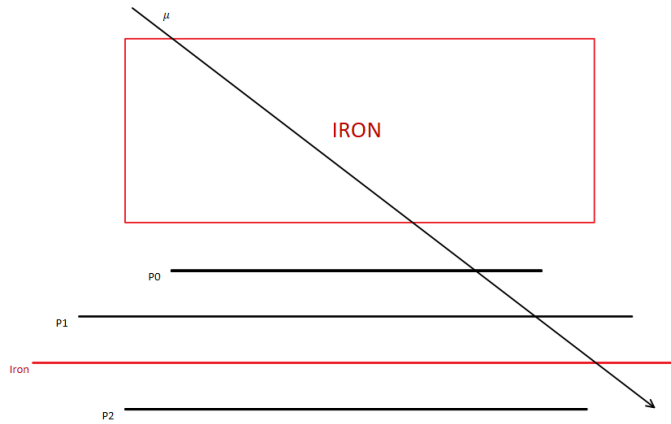


Figure 5.1: Scematic of an escaping muon being detected by planes P0 and P1, but not P2 and therefore resulting in a fake trigger signal.

case the time measurement starts without a stopped muon. This can affect the measurement in two different ways: Firstly, no other particle passes and thus only overflow values are generated. Secondly a background signal triggers a channel and produces a fake event.

Another possible reason of background is the correct detection of a stopping muon but the electron is not detected, because it leaves the detector or it does not have enough energy to leave the iron block. This case is shown in Figure 5.2. And again this leads either to an overflow value or to a fake event because of a background signal. These background events can not be eliminated since this experiment does not

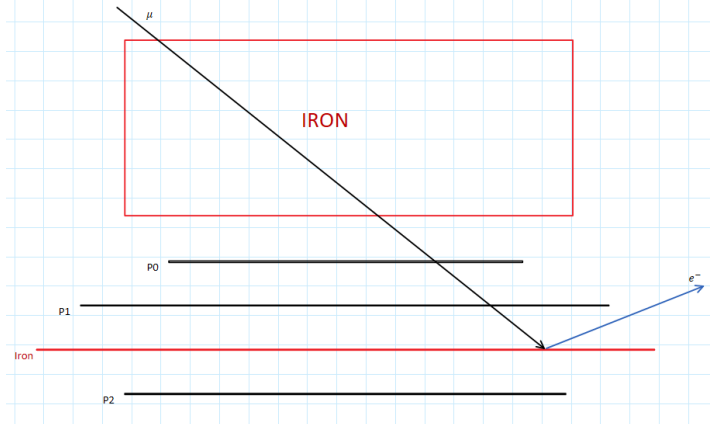


Figure 5.2: Schematic of an escaping electron after a muon has been stopped. The direction of the decay products is random, therefore the electron can escape the detector.

determine the type of the particle.

To handle the analysis first all planes were looked at separately. This step ensures the statistical independency of all planes, especially of P0 and P1 of which signals often correlate. In the end all independent analysis are combined for a final result.

At first all overflow values have to be eliminated from the data set. The entry for each single plane is considered valid if it has a non overflow value in the TDC and is only detected in this plane.

5.2 Fit function

Particle decay at rest is, like every natural spontaneous process, a Poisson distributed process. So the probability for a decay after a given time t is represented by a negative exponential probability function like

$$N(t) = a \cdot \exp\left(-\frac{t}{\tau}\right)$$

where N is the number of particles and τ the decay rate.

As discussed before background has to be taken into consideration. Since there is no reason to assume the background signals vary over time, the distribution of the background will be considered to be flat. Thus, the complete fit function is

$$N(t) = a \cdot \exp\left(-\frac{t}{\tau}\right) + b \quad (5.1)$$

with the parameter a as a scale factor representing the total amount of particles at $t = 0$ ($a = N(0)$) and b representing the constant offset due to background signals. The aim of this analysis is to find the muon mean lifetime τ . To do this the fit function will be applied to the data of the planes using the Python package *scipy* [4].

Furthermore, the first few bins will be excluded from these analysis to reduce the effects of muon capture which will be discussed in section 5.4.

5.3 Fit results

At first only all single planes will be analyzed separately after which all data is taken into account for the final result. All fit results however are shown in Table 5.1 for a quick overview of the findings. For this analysis, data from 0 ns to 8700 ns is taken into account.

In the first plane P0 the lowest number of events could be detected which reflects on the resulting lifetime, which is the furthest away from the actual value and having the biggest χ^2 -test value. For P0 a total of 48 bins meaning each bin represents 181.25 ns, while the fit is conducted in the interval 725 ns to 8700 ns. The data and the fitted function for P0 are shown in Figure 5.3.

The plane P1 measured 2345 events resulting in the lowest χ^2 -test value per degree of freedom. For this

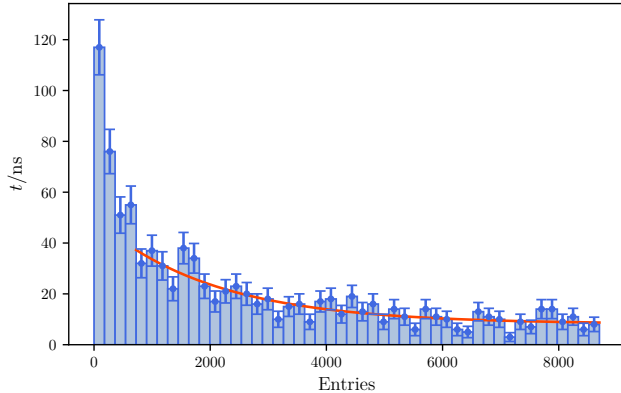


Figure 5.3: Measured events in the plane P0 with plotted decay function.

plane 77 bins where used with bin sizes of 113 ns. The implementation of the fit function starts at 226 ns. The data and the plotted fit function are shown in Figure 5.4.

For the last plane P2, 60 bins with 145 ns are used in the analysis. The fit is conducted beginning at 435 ns. Both data and plotted fit function are shown in Figure 5.5.

Lastly all of the above selected events are considered to gain the highest possible statistic. Thus, a total amount of 5885 events is taken into consideration. For this analysis 44 bins each representing 198 ns are used. The fit is done for times greater than 593 ns. The sum of all selected data and the corresponding fit are shown in Figure 5.6. The final result is

$$\tau = (2.1 \pm 0.1) \mu\text{s}.$$

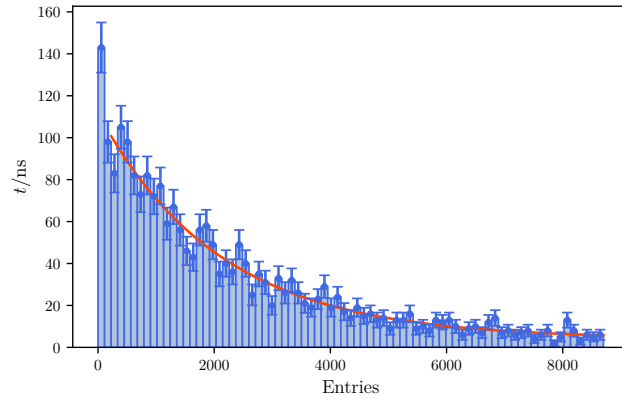


Figure 5.4: Measured events in the plane P1 with plotted decay function.

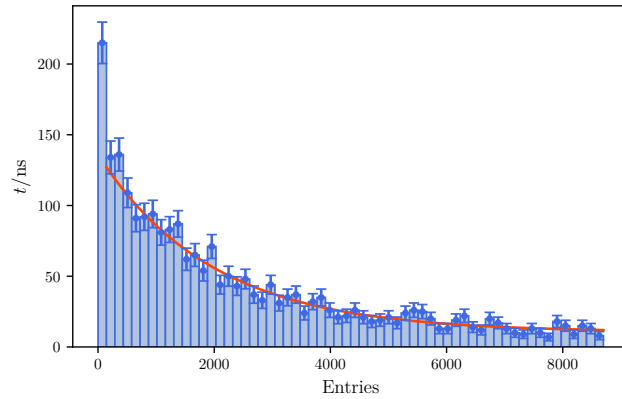


Figure 5.5: Measured events in the plane P2 with plotted decay function.

Table 5.1: Parameters of all data analysis fits.

| Plane | Entries | Parameter a | Parameter b | Lifetime $\tau/\mu\text{s}$ | $\chi^2/\text{d.o.f.}$ |
|--------------|---------|---------------|---------------|-----------------------------|------------------------|
| P0 | 1030 | 41 ± 5 | 8 ± 2 | 2.0 ± 0.4 | 1.085 |
| P1 | 2345 | 108 ± 3 | 4 ± 1 | 2.1 ± 0.1 | 0.893 |
| P2 | 2510 | 125 ± 5 | 10 ± 2 | 2.0 ± 0.1 | 0.923 |
| P1 + P2 + P3 | 5885 | 400 ± 11 | 30 ± 4 | 2.1 ± 0.1 | 0.959 |

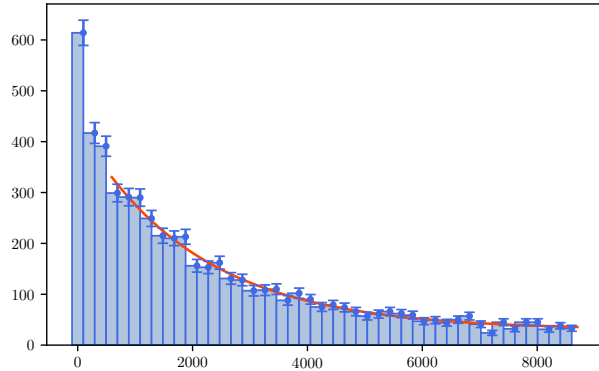


Figure 5.6: Measured events in all planes with plotted decay function.

5.4 Decay of captured muons

Since the muon has apart from its mass the same features as an electron, there is a probability for atoms capturing negative muons which can influence the outcome of this experiment as discussed before. This affects the decay time of the muon due to quantum mechanic effects:

Since the muon is in a bound state and thus under the influence of binding energy, the phase space for the decay gets reduced. A second effect is the relativistic time dilation due to the orbital movement of the muon. Both of these effects lead to a reduction of the decay rate of the bound state compared to the free state of the muon. A third effect is the Compton effect of the emitted electron, which can (virtually) interact with the atomic nucleus and therefore increases the decay rate of the bound muon compared to free muons. Considering these effects, the decay time for bound muons has to be modified[2].

The time intervall measured by this experiment also covers the area of times of the decay of captured muons in iron atoms which is $\tau_{\text{iron}} = 0.206 \mu\text{s}$. Only negative muons can get captured by the iron atoms, so for simplicity reasons this analysis assumes that all positive muons decay freely, while most negative muons are captured by the material. Because of this the fit function 5.1 can be adapted to

$$N(t) = a \cdot \left(\frac{N_+}{N_-} \exp\left(-\frac{t}{\tau_+}\right) + \exp\left(-\frac{t}{\tau_-}\right) \right) + b$$

where τ_+ is the decay time of the free decaying positive muons and τ_- is the decay time of the captured negative muons. The fraction $\frac{N_+}{N_-}$ describes the rate of positive muons over negative muons reaching the surface of the earth. In this analysis this value will be assumed to be $\frac{N_+}{N_-} \approx 1.2$ [1]. To have the most statistic the events of all planes in 59 bins will be used. The used event data and the plotted fit is shown in Figure 5.7. The calculated fit parameter are

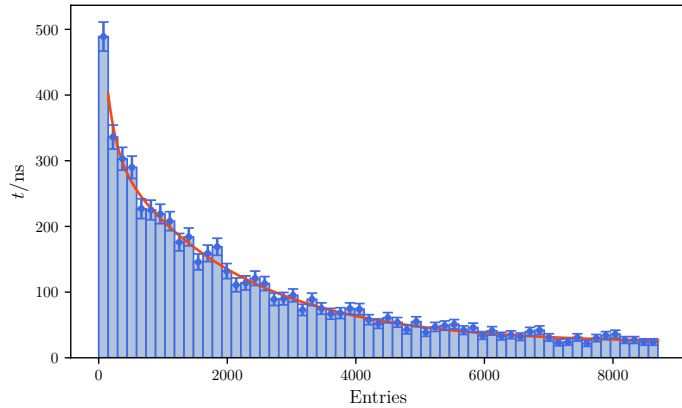


Figure 5.7: Measured events in all planes with plotted modified decay function for captured muons.

$$\begin{aligned}
 a &= 255 \pm 11 \\
 b &= 22 \pm 2 \\
 \tau_+ &= (1.9 \pm 0.1) \mu\text{s} \\
 \tau_- &= (0.15 \pm 0.04) \mu\text{s}
 \end{aligned}$$

with a test value of $\chi^2 = 0.89$ per degree of freedom.

Chapter 6

Final Results and Conclusions

In this report a plastic scintillator made up of three planes in combination with a basic trigger system was used to detect stopping cosmic muons and their lifetime. From the total of 1184834 measured trigger events only 5885 resulting in an efficiency value of

$$\epsilon = \frac{5885}{1184834} \approx 5 \cdot 10^{-3}.$$

This efficiency is far from optimal but was to be expected given the amount of possible fake signals and other background signals. Using the fit on the available data a mean muon lifetime could be estimated as

$$\tau = (2.1 \pm 0.1) \mu\text{s}.$$

This calculated value deviates 4.4% of the literature value of $\tau_{\text{pdg}} = 2.1969811 \pm 0.0000022$ [6]. Since the relative deviation is small and the true value well inside the standard deviation and therefore consistent with it, this measurement will be considered successful.

Furthermore, an attempt to calculate the lifetime of bound muons in iron was made. The analysis results in a lifetime of

$$\tau_{\text{bound}} = (0.15 \pm 0.04) \mu\text{s},$$

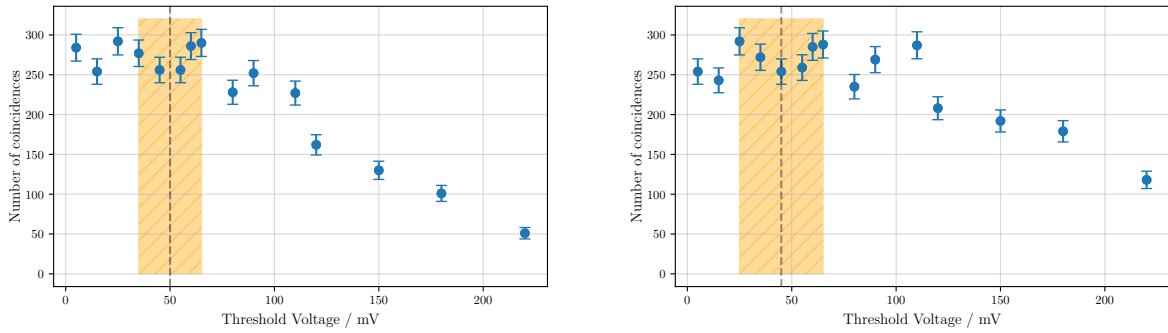
which deviates 27.2% of the experimental value of $\tau_{\text{bound}} = 0.206 \mu\text{s}$ [1]. Since the effect of the decay of captured muons is much smaller than the effect of free muons, more measured events would be needed to improve this measurement to eventually become valid and consistent.

Bibliography

- [1] N. Agafonova et al. “The muon decay and muon capture detection with LVD”. In: *Book of Abstracts* (2006), p. 201.
- [2] Robert W Huff. “Decay rate of bound muons”. In: *Annals of Physics* 16.2 (1961), pp. 288–317. doi: [https://doi.org/10.1016/0003-4916\(61\)90039-2](https://doi.org/10.1016/0003-4916(61)90039-2).
- [3] The pandas development team. *pandas-dev/pandas: Pandas*. Version latest. Feb. 2020. doi: 10.5281/zenodo.3509134.
- [4] Pauli Virtanen et al. “SciPy 1.0: Fundamental Algorithms for Scientific Computing in Python”. In: *Nature Methods* 17 (2020), pp. 261–272.
- [5] J.D. Wrbanek and S.Y. Wrbanek. *Space Radiation and Impact on Instrumentation Technologies*. 2020.
- [6] P.A. Zyla et al. “Review of Particle Physics”. In: *PTEP* 2020.8 (2020). and 2021 update. doi: 10.1093/ptep/ptaa104.

Appendix A

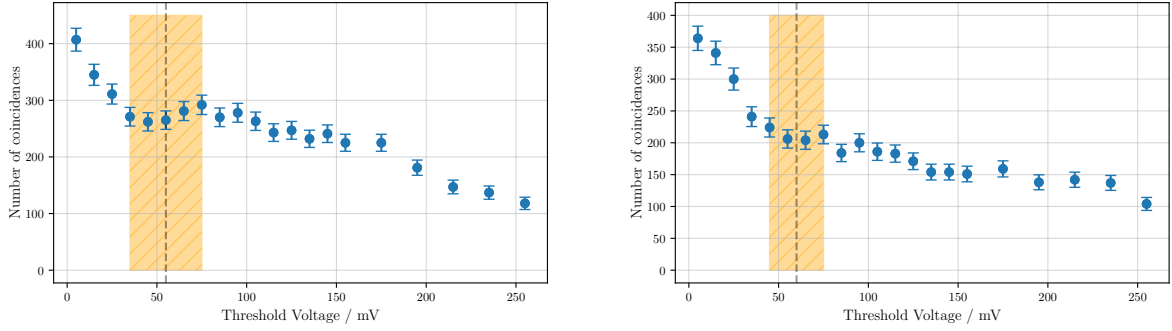
Threshold voltages of the PMTs



(a) Data of the R00 signal. The central value of the plateau is 50 mV.

(b) Data of the second measurement of the R10 signal. The central value of the plateau is 45 mV.

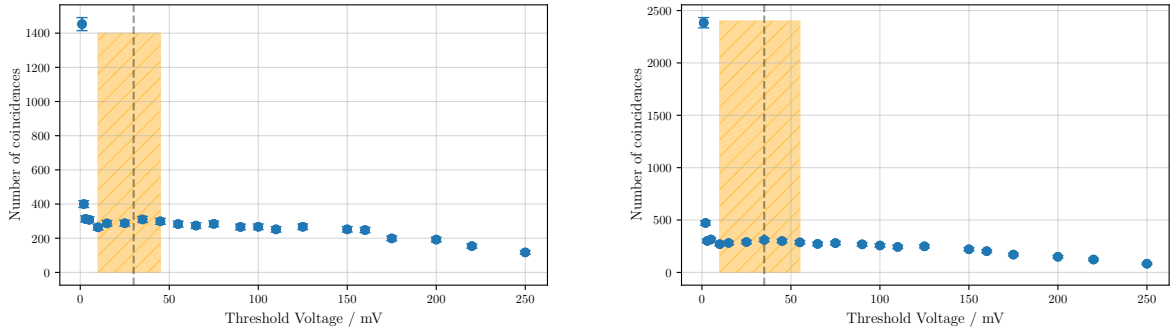
Figure A.1: Measured number of coincidences concerning varying threshold voltages of the R00 and R10 PMTs. The dashed line indicates the central values of each plateau. The striped orange areas mark the found plateaus.



(a) Data of the R01 PMTs. The central value of the plateau is 55 mV.

(b) Data of the R11 PMTs. The central value of the plateau is 60 mV.

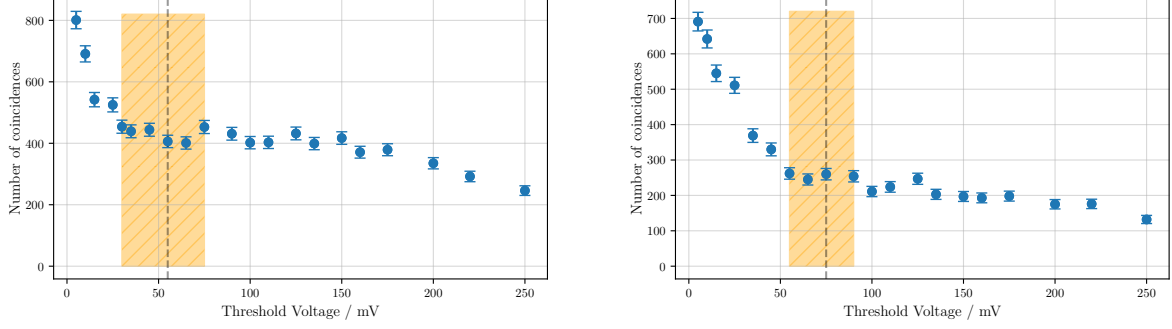
Figure A.2: Measured number of coincidences concerning varying threshold voltages of the R01 and R11 PMTs. The dashed line indicates the central values of each plateau. The striped orange areas mark the found plateaus.



(a) Data of the L00 PMTs. The central value of the plateau is 30 mV.

(b) Data of the L10 PMTs. The central value of the plateau is 35 mV.

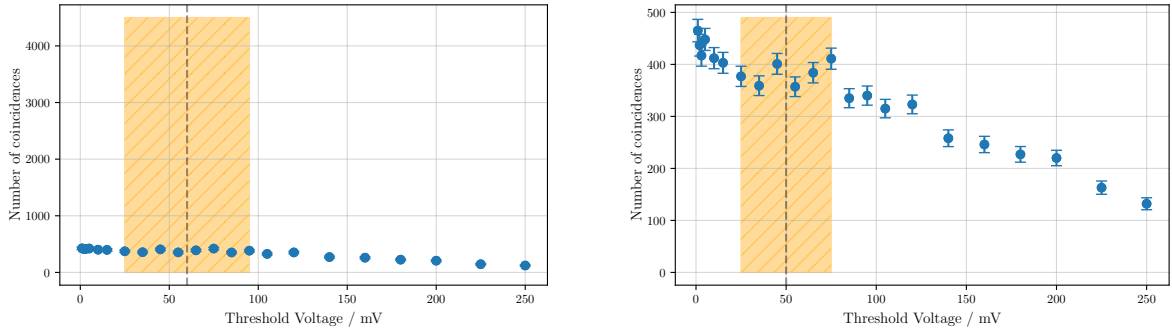
Figure A.3: Measured number of coincidences concerning varying threshold voltages of the L00 and L10 PMTs. The dashed line indicates the central values of each plateau. The striped orange areas mark the found plateaus.



(a) Data of the L01 PMTs. The central value of the plateau is 55 mV.

(b) Data of the L11 PMTs. The central value of the plateau is 75 mV.

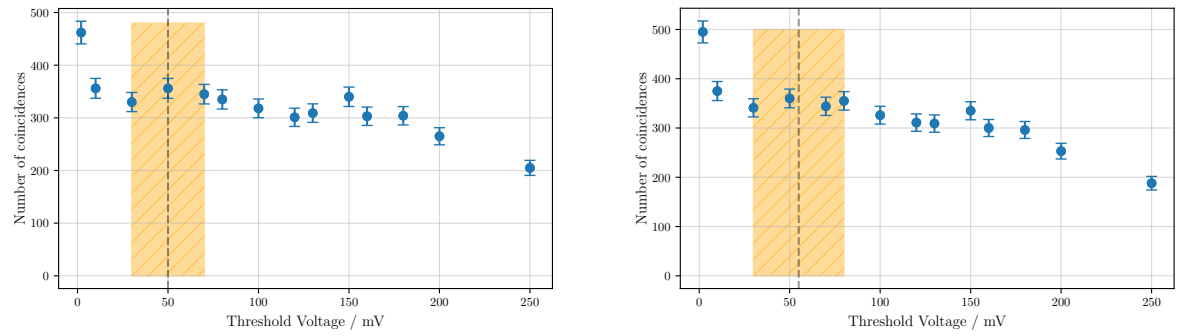
Figure A.4: Measured number of coincidences concerning varying threshold voltages of the L01 and L11 PMTs. The dashed line indicates the central values of each plateau. The striped orange areas mark the found plateaus.



(a) Data of the second measurement of the L10 PMTs. The central value of the plateau is 60 mV.

(b) Data of the L20 PMTs. The central value of the plateau is 50 mV.

Figure A.5: Measured number of coincidences concerning varying threshold voltages of the L10 and L20 PMTs. The dashed line indicates the central values of each plateau. The striped orange areas mark the found plateaus.



(a) Data of the L21 PMTs. The central value of the plateau is 50 mV.

(b) Data of the R21 PMTs. The central value of the plateau is 55 V.

Figure A.6: Measured number of coincidences concerning varying threshold voltages of the L21 and R21 PMTs. The dashed line indicates the central values of each plateau. The striped orange areas mark the found plateaus.

Appendix B

TDC calibrations

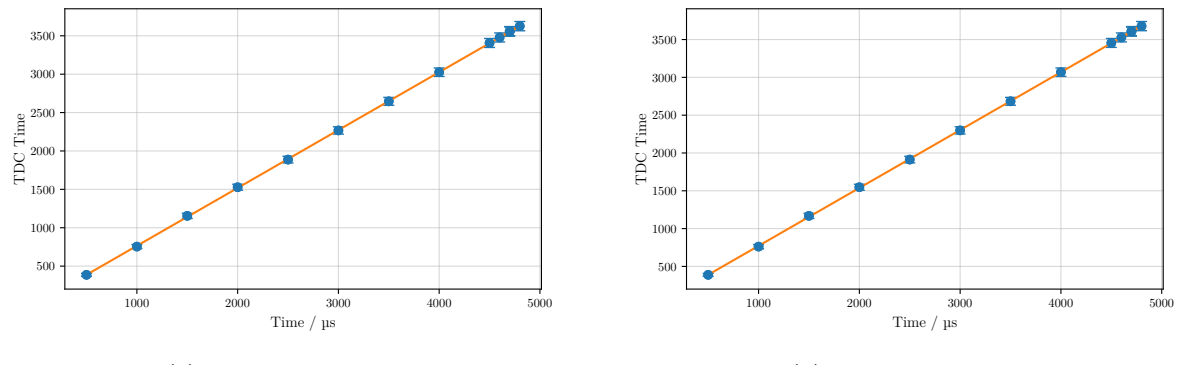
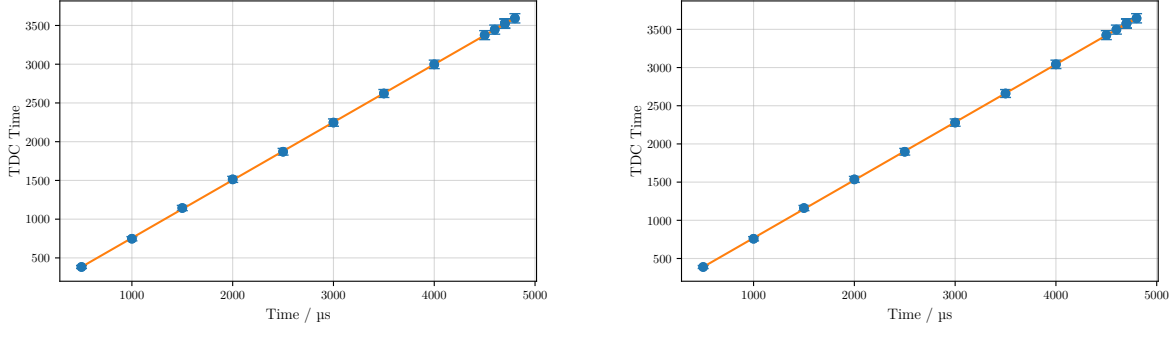
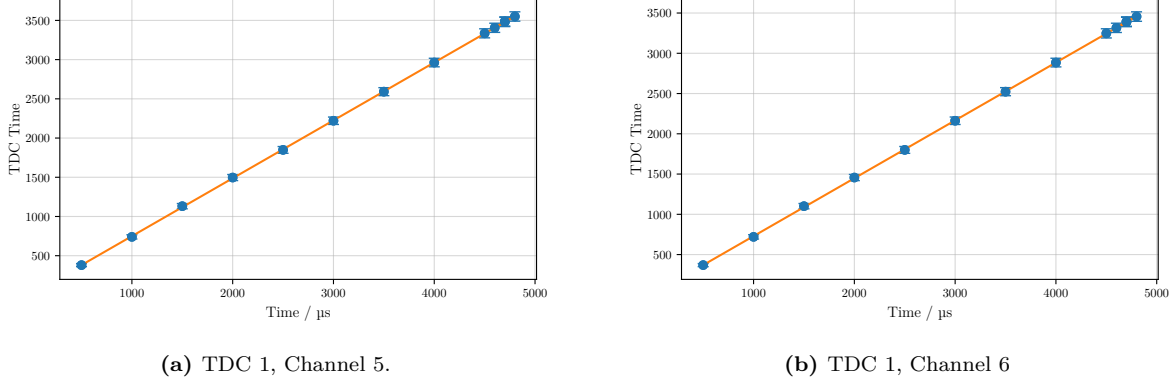


Figure B.1: Calibration Fits of Channel 1 and 2 of TDC 1.



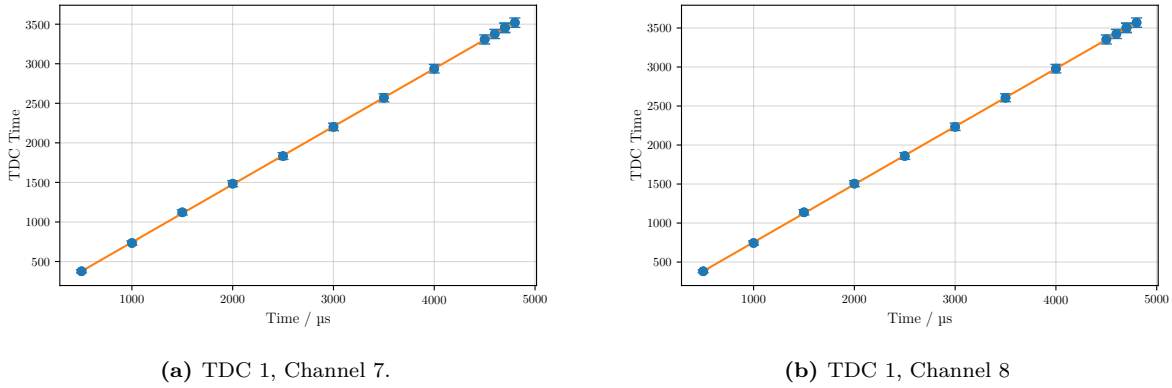
(a) TDC 1, Channel 3.

(b) TDC 1, Channel 4

Figure B.2: Calibration Fits of Channel 3 and 4 of TDC 1.

(a) TDC 1, Channel 5.

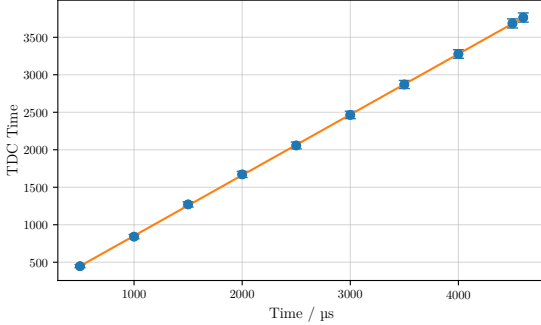
(b) TDC 1, Channel 6

Figure B.3: Calibration Fits of Channel 5 and 6 of TDC 1.

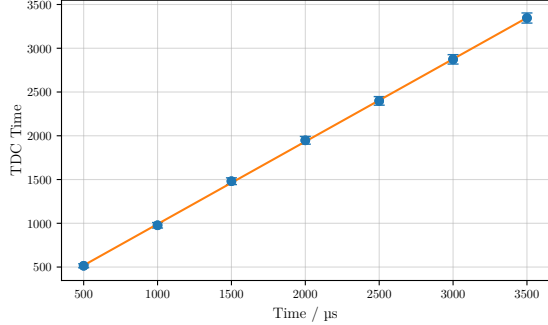
(a) TDC 1, Channel 7.

(b) TDC 1, Channel 8

Figure B.4: Calibration Fits of Channel 7 and 8 of TDC 1.

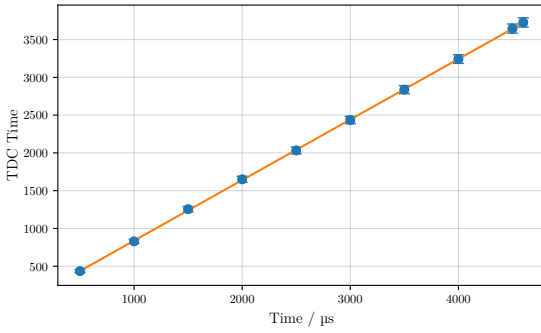


(a) TDC 2, Channel 1.

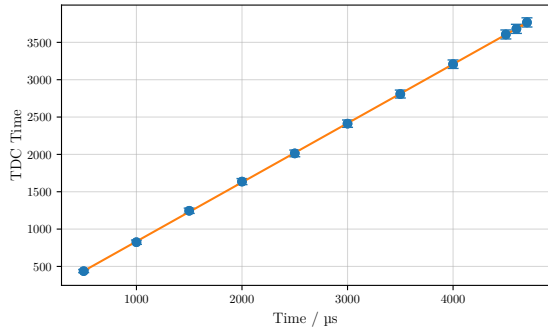


(b) TDC 2, Channel 2

Figure B.5: Calibration Fits of Channel 1 and 2 of TDC 2. Range of Channel 1 is limited to $4.6\text{ }\mu\text{s}$ and range of Channel 2 is limited to $3.5\text{ }\mu\text{s}$.

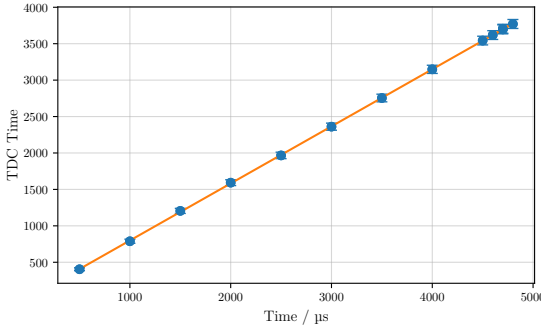


(a) TDC 2, Channel 3.

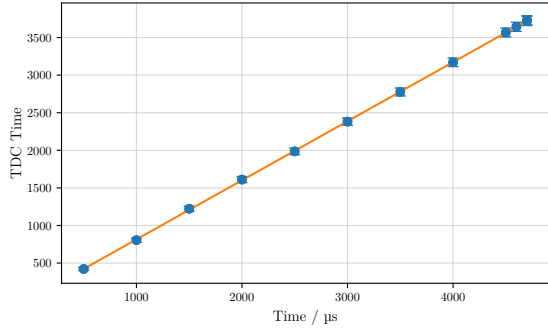


(b) TDC 2, Channel 4

Figure B.6: Calibration Fits of Channel 3 and 4 of TDC 2. Range of Channel 3 is limited to $4.6\text{ }\mu\text{s}$ and range of Channel 4 is limited to $4.7\text{ }\mu\text{s}$.



(a) TDC 2, Channel 5.



(b) TDC 2, Channel 6

Figure B.7: Calibration Fits of Channel 5 and 6 of TDC 2. Range of Channel 6 is limited to $4.8\text{ }\mu\text{s}$.

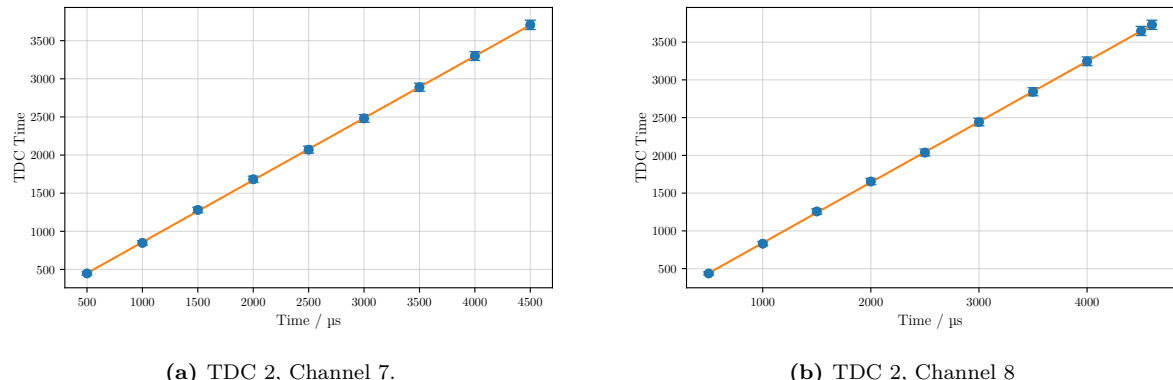


Figure B.8: Calibration Fits of Channel 7 and 8 of TDC 2. Range of Channel 7 is limited to $4.5\text{ }\mu\text{s}$ and range of Channel 8 is limited to $4.6\text{ }\mu\text{s}$.